Applied Catalysis A, General 720 (2026) 120976

Contents lists available at ScienceDirect

Applied Catalysis A, General

journal homepage: www.elsevier.com/locate/apcata

Tailoring reaction path in CO_2 hydrogenation to methanol by selective Zr or Ce doping of CoIn catalysts

Xia Li [a], Christopher Foo [b], Xinlin Hong [a,*], Guangchao Li [c,d,e,*]

[a] College of Chemistry and Molecular Sciences, Wuhan University, Wuhan 430072, China
[b] Diamond Light Source, Harwell Science and Innovation Campus, Fermi Ave, Didcot, UK
[c] Department of Applied Biology and Chemical Technology, The Hong Kong Polytechnic University, 999077, Hong Kong, China
[d] PolyU-Daya Bay Technology and Innovation Research Institute, The Hong Kong Polytechnic University, Huizhou 516081, China
[e] The Hong Kong Polytechnic University Shenzhen Research Institute, The Hong Kong Polytechnic University, Shenzhen 518057, China

ARTICLE INFO

Keywords:
CoIn-based catalysts
ZrO_2 and CeO_2 dopants
CO_2 Hydrogenation
Methanol synthesis

ABSTRACT

The hydrogenation of CO_2 to methanol represents a pivotal route for carbon capture and utilization, yet designing catalysts that concurrently achieve high activity and selectivity remains challenging. This work explored the promotional effects of ZrO_2 and CeO_2 on CoIn-based catalysts for the CO_2 hydrogenation to methanol reaction. While both dopants improve catalytic performance, they exert distinct structural and mechanistic roles. ZrO_2 doping primarily enhances CO_2 conversion by facilitating the formate pathway with a reduced energy barrier. In contrast, CeO_2 incorporation enables high and stable methanol yields even under harsh conditions, due to the dual-pathway mechanism involving formate and CO intermediates. The study establishes that targeted doping is a powerful lever for engineering reaction networks in In_2O_3 catalysts, providing a clear design principle for advancing CO_2 hydrogenation.

1. Introduction

The increasingly severe global climate change and growing energy demands are driving our focus towards carbon capture and utilization technologies [1–4]. Among these, CO_2 hydrogenation to value-added fuels and chemicals, such as methanol, is regarded as a highly promising green chemistry pathway. Methanol serves not only as an important chemical feedstock but also as an ideal liquid energy carrier [5–7]. However, the core challenges of this reaction lie in the inherent chemical stability of the CO_2 molecule and the competition from the the Reverse Water-Gas Shift (RWGS) reaction [8,9]. These factors make it difficult to develop catalyst systems that simultaneously achieve high methanol selectivity and high CO_2 conversion.

Among the various catalysts developed for CO_2 hydrogenation to methanol, copper-based systems such as the conventional Cu/ZnO/Al_2O_3 catalyst have achieved industrial application [10–12]. However, they are still hampered by issues like inadequate thermal stability and a tendency to sinter and deactivate [13,14]. In recent years, In_2O_3-based catalysts have attracted widespread attention due to their near-perfect selectivity towards methanol [15–17]. Although pure In_2O_3 possesses a low oxygen vacancy formation energy, which facilitates CO_2 adsorption and activation, its CO_2 hydrogenation activity remains limited, resulting in a low methanol yield [18–21]. To further improve the catalytic activity, noble metals such as Pd [21,22], Pt [23], Rh [24] and Au [25] are often employed to form intermetallic compounds with In_2O_3, thereby promoting H_2 dissociation. For example, Wang et al. screened a series of transition metals (Cr, Mn, Fe, Co, Ni, Cu, Zn, and Ga) doped in In_2O_3 catalysts and found that the composite with cost-effective Co_3O_4 exhibited superior activity [26]. This enhancement was attributed to the CoO_x–InO_x interface, which not only increased oxygen vacancy density but also promoted the dissociative adsorption of H_2. However, while Co promotes hydrogen dissociation, it still retains some methanation activity, leading to the formation of methane by-products and restricting further improvement in methanol selectivity [27,28]. Thus, rationally regulating the electronic structure and surface properties of CoIn catalysts becomes crucial for achieving a breakthrough in their performance.

Introducing dopant elements is a widely recognized strategy for modulating the electronic structure and surface properties of host catalysts. Given that In_2O_3-based catalysts utilize oxygen vacancies as active sites, ZrO_2 and CeO_2 emerge as highly attractive dopants owing to their exceptional redox activity. ZrO_2, as an amphoteric oxide, is often

* Corresponding author at: Department of Applied Biology and Chemical Technology, The Hong Kong Polytechnic University, 999077, Hong Kong, China.
E-mail address: guangchao.li@polyu.edu.hk (G. Li).

https://doi.org/10.1016/j.apcata.2026.120976
Received 4 January 2026; Received in revised form 17 March 2026; Accepted 17 April 2026
Available online 20 April 2026

used as a support or promoter to enhance CO_2 adsorption and activation [29–32]. Research indicates that introducing In-O_V-Zr sites into the system by supporting In_2O_3 on m-ZrO_2 or forming In_2O_3-ZrO_2 solid solution helps suppress the excessive reduction of In_2O_3 and enhances CO_2 adsorption capacity [33,34]. Meanwhile, CeO_2 plays a key role in redox reactions due to its excellent oxygen storage capacity and ability to form oxygen vacancies [35,36]. For the In_2O_3-Co_3O_4 catalyst, Ke et al. revealed that the introduction of Ce leads to unique oxygen vacancies over the CeO_2 surface upon H_2 reduction. These vacancies can effectively capture CO_2, thereby enhancing the hydrogenation activity [37]. Besides, Zhu et al. found that Ce on Cu-Zn-Ce catalysts promotes the coverage of formate species on the copper surface and accelerates the subsequent hydrogenation of CO intermediates, thereby inhibiting the RWGS reaction [38]. Although studies have explored the impact of single dopants on catalyst performance, there is currently a lack of clear understanding and in-depth comparative research on how dopants with different characteristics precisely regulate the reaction pathways of CoIn catalysts and ultimately determine the differences in the conversion and selectivity.

In this work, we investigated the effects of incorporating ZrO_2 or CeO_2 on CoIn catalysts for CO_2 hydrogenation to methanol. The introduction of ZrO_2 primarily enhances the CO_2 conversion compared to the pristine CoIn catalyst, following a singular formate pathway. In contrast, the incorporation of CeO_2 notably boost both CO_2 conversion and methanol selectivity. Mechanistic insights reveal that Ce-containing catalysts activate both formate and CO pathways, leading to optimized and balanced reaction kinetics. This work demonstrates that precisely doping to regulate reaction routes is an effective strategy for efficient CO_2 conversion to methanol, providing key guidance for designing advanced In_2O_3-based catalysts.

2. Results and discussion

2.1. Catalyst structural characterization

To compare the doping effects of Zr and Ce, we synthesized CoIn-based catalysts involving CoIn, CoInZr, and CoInCe. All samples were prepared via the coprecipitation method, with a fixed Co/In molar ratio of 2:1 and a doping element (Zr or Ce) content of 10 wt.%. The crystal structures of the catalysts were characterized by X-ray diffraction (XRD). In Fig. 1a, the fresh catalysts exhibit distinct diffraction peaks at 30.6° and 35.6°, which are indexed to the (222) and (400) Miller planes of cubic In_2O_3 (PDF #06–0416) [39]. Additionally, two weak diffraction peaks observed at around 19.0° and 36.8° can be assigned to the (111) and (311) planes of Co_3O_4 (PDF #43–1003). For the CoInCe catalyst, characteristic peaks of CeO_2 (PDF #43–1002) are also detected at 28.5° and 33.0°, confirming the successful incorporation of CeO_2. In contrast, no discernible ZrO_2 diffraction signals are observed in the CoInZr, which may be attributed to either the ZrO_2 crystallite size below 5 nm or the presence of amorphous ZrO_2, both of which are beyond the XRD detection limit. Comparative analysis reveals that the FWHM of In_2O_3 in CoIn is smaller than that in CoInZr and CoInCe. This indicates that Ce and Zr interact with In_2O_3, thereby suppressing the sintering and agglomeration of In_2O_3 [40]. To investigate the structural evolution during the CO_2 hydrogenation, XRD analysis was also performed on reduced and spent catalysts (samples reduced in 5% H_2/Ar for 2 h are labeled as "re-" (Fig. 1a), while the spent catalysts after reaction are denoted as "sp-"(Fig. S1)). The characteristic diffraction peaks of Co_3O_4 completely disappear in all reduced samples, and a new peak emerges at 44.2°, corresponding to the (111) plane of metallic Co (PDF #15–0806), confirming the reduction of Co_3O_4 to Co (Fig. 1a). The XRD patterns of the spent catalysts are similar to those of the reduced catalysts, indicating that the crystalline structure remains stable under reaction conditions (Fig. S1). Notably, the crystallite sizes of In_2O_3 in the reduced

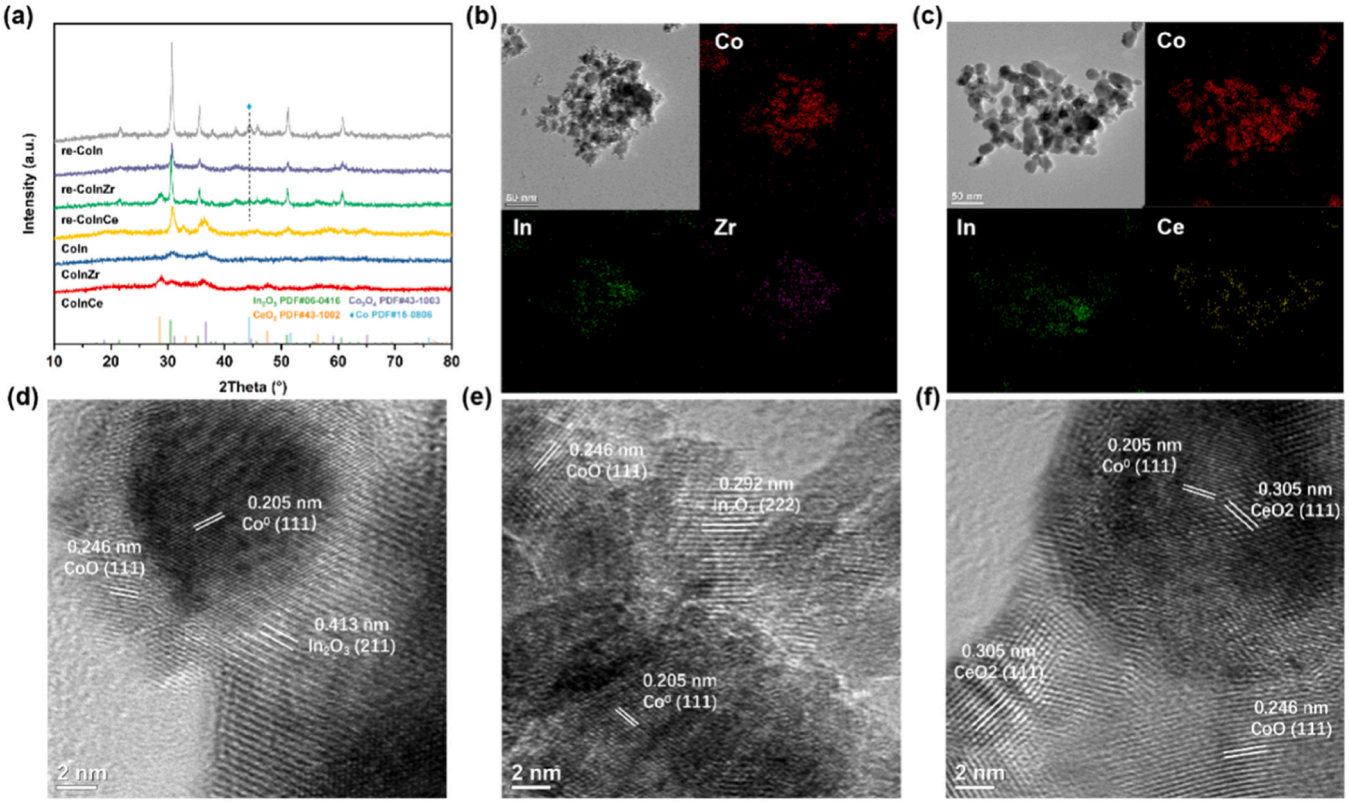

Fig. 1. Structure and morphology of CoIn-Based Catalysts. (a)XRD patterns of fresh and reduced CoIn, CoInZr, and CoInCe. TEM image for (b) spent CoInZr and (c) spent CoInCe with corresponding elemental mapping. HRTEM images of the (d) spent CoIn, (e) CoInZr, and (f) CoInCe.

catalysts, calculated using the Scherrer equation, follow the order: re-CoIn > re-CoInCe > re-CoInZr, which is consistent with the trend observed for metallic Co (Table S1). This may be due to ZrO_2 or CeO_2 inhibiting the reduction of Co_3O_4 to Co^0.

Nitrogen adsorption-desorption was used to measure the surface area and pore size distribution of CoIn-based catalysts. All catalysts showed type IV isothermal curves and H1 hysteresis loops, confirming they are mesoporous materials (Fig. S2-S3) [41]. Notably, CoInZr and CoInCe, both before and after the reaction, had larger surface areas than CoIn (Table S2). This matches the XRD results, indicating that adding Zr or Ce reduces the crystallite sizes, which exposes more active sites. Furthermore, the morphology and nanostructure of the samples were imaged by TEM. Fig. S4 demonstrates that all fresh samples exhibit a layered structure of stacked nanosheets, and the morphology remains unchanged by doping with either ZrO_2 or CeO_2. High-resolution TEM images show the lattice fringes of Co_3O_4, In_2O_3, and CeO_2, in agreement with the XRD results (Fig. S5). Meanwhile, elemental mapping indicates that Co, In, and the dopant elements (Zr, Ce) exhibit highly uniform distribution throughout the catalyst (Fig. S6). After the reaction, the catalyst morphology underwent remarkable reconstruction, transforming from a sheet-like structure into a spherical form, likely due to sintering at elevated temperatures (Fig. 1b, 1c, S4 and S7). Additionally, phase separation behavior is observed in the three spent catalysts. Lattice fringes of approximately 0.205 nm are observed in the centre of the spherical structure, attributed to the (111) crystal plane of Co (Fig. 2d-f). The average particle sizes of CoInZr, CoInCe and CoIn are 9 nm, 15 nm, and 17.5 nm, respectively, indicating that Zr and Ce effectively suppress the agglomeration of Co (Fig. S4). Furthermore, In_2O_3 and CoO are also detected in the spent samples. Previous reports pointed out that this structure facilitates the surface enrichment of In_2O_3, promoting its high dispersion and generating additional oxygen vacancies [42]. This explains the superior activity of CoIn catalysts compared to pure In_2O_3.

2.2. Catalytic performances

To comprehensively evaluate the catalyst performance, the CO_2 hydrogenation activity was tested at at 250–330 °C, 5 MPa, and a WHSV of 21600 mL $gcat^{-1}$ h^{-1} (Fig. 2a-c and Table S3). As shown in Fig. 2b and S8, while the hydrogenation products of pure In_2O_3 were limited to CO and methanol, the CoIn-based catalysts yielded alkanes, CO, and methanol, suggesting that Co introduction facilitates CH_4 production. Since methanol synthesis is exothermic while RWGS reaction is endothermic [43,44], the CO_2 conversion of all three catalysts increased with rising temperature, whereas methanol selectivity gradually decreased (Fig. 2a). Notably, for CoInCe, the methanol selectivity decreased by only about 3% per 20 °C increase below 310 °C, indicating that CoInCe was less affected by temperature than CoIn and CoInZr. Consequently, the space-time yield (STY) of methanol over CoIn and CoInZr exhibited a volcanic trend with temperature, reaching a maximum at 310 °C (Fig. 2c). In contrast, for CoInCe, the STY continued to increase from 647.7 to 738.6 mg $gcat^{-1}$ h^{-1} as the temperature rose from 310 °C to 330 °C. At 310 °C, the STY of CoInZr and CoInCe increased by 30% compared to CoIn, indicating that ZrO_2 and CeO_2 played a positive role in enhancing the catalytic activity for CO_2 hydrogenation to methanol. Moreover, although CoInZr and CoIn showed similar trends in STY variation, the methanol yield of CoInZr was consistently higher than that of CoIn. This can be attributed to the higher CO_2 conversion of CoInZr under identical reaction conditions, while the methanol selectivity of the two catalysts remained nearly the same. It is noteworthy that all three catalysts demonstrated excellent stability during testing over 100 h, with no significant decline in activity or selectivity observed (Fig. 2e).

The difference in catalytic activity was quantitatively evaluated by determining the apparent activation energies (*Ea*) (Fig. 2d). Kinetic analysis based on the Arrhenius equation revealed that the *Ea* value for CoInZr (40.5 kJ mol^{-1}) was much lower than that for CoIn

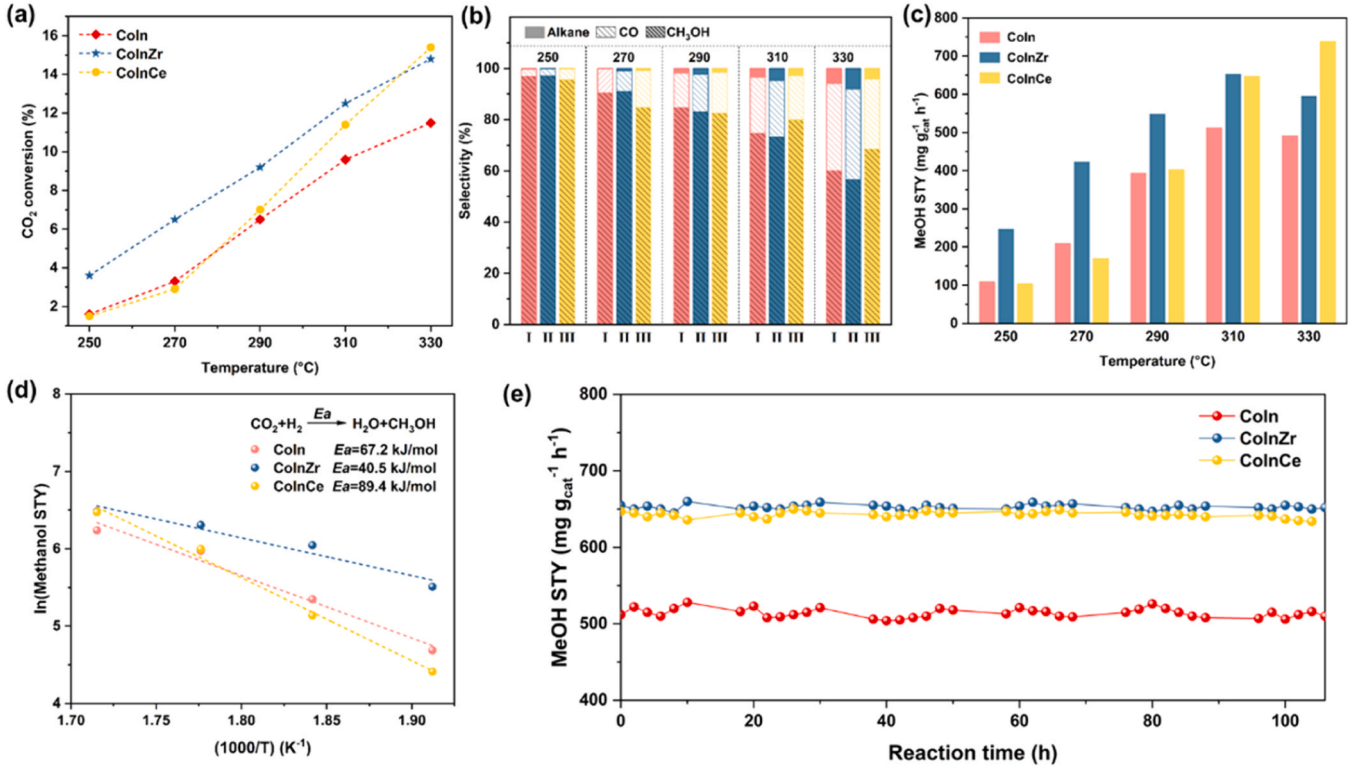

Fig. 2. Catalytic performance of CoIn, CoInZr, and CoInCe in the CO_2 hydrogenation reaction. (a) CO_2 conversion of CoIn, CoInZr, and CoInCe. (b) Product distribution and selectivity of CoIn (I), CoInZr (II), and CoInCe (III). (c) Relationship between the space-time yield (STY) of methanol and the reaction temperature. (d) Arrhenius plots for the methanol synthesis reaction kinetics and the corresponding activation energy (*Ea*) calculations by using the Arrhenius equation. (e) Catalytic stability of CoIn, CoInZr, and CoInCe, Reaction conditions: 0.1 g catalyst, WHSV = 21600 mL g_{cat}^{-1} h^{-1}, 5 MPa, 310 °C, $H_2/CO_2 = 3$.

(67.2 kJ mol^{-1}). This kinetic evidence clearly demonstrates that Zr doping effectively lowered the reaction energy barrier for CO_2 hydrogenation to methanol, potentially by optimizing reactant adsorption and stabilizing key intermediates, thereby enhancing the catalytic activity. Notably, CoInCe displayed a considerably higher *E*a of 89.4 kJ mol^{-1} . Generally, an increase in *E*a suggests the presence of higher-energy transition states or stronger energy barriers along the reaction pathway. Combined with its superior methanol selectivity in the higher temperature range, the elevated *E*a value of CoInCe implies that it may follow a reaction mechanism distinct from those of CoIn and CoInZr [45].

2.3. Surface properties investigation

H_2 Temperature-Programmed Reduction (H_2-TPR) was applied to analyze the reduction behavior of the catalysts. All catalysts exhibited three distinct reduction regions in their H_2-TPR profiles (Fig. 3a). The β region corresponds to the reduction of surface CoO_x species to metallic Co, while the γ region is attributed to the reduction of bulk In_2O_3 [46, 47]. In contrast, the reduction process in the low-temperature α region is more complex. Between 180 and 330 °C, the observed reduction peak involves the transformation of Co^{3+} to Co^{2+} concurrent with the partial reduction of surface In species [40,48]. A comparison of the reduction profiles shows that the reduction of Co_3O_4 proceeds in a similar temperature range (300–310 °C) both with and without ZrO_2, indicating that Zr has a minimal influence on the reduction of Co_3O_4 (Fig. S9). The shift of the reduction peak for the CoInZr towards lower temperatures may be attributed to ZrO_2 promoting the surface reduction of In_2O_3 [49]. This reduction behavior contributes to an increased concentration of surface oxygen vacancies. Furthermore, two reduction peaks are observed in the β region: the low-temperature peak corresponds to the reduction of CoO_x species interacting with In species, whereas the high-temperature peak is associated with the reduction of isolated CoO_x species [40]. Peak integration of the β region revealed that the area proportion corresponding to Co_3O_4 reduction to CoO_x is significantly higher for CoInZr and CoInCe than for CoIn (Fig. S10 and Table S4). This indicates that both dopants fostered a higher proportion of CoO_x species in intimate contact with InO_x, thus preserving richer CoO_x-InO_x interfaces and promoting CO_2 hydrogenation to methanol.

CO_2 Temperature-Programmed Desorption (CO_2-TPD) was employed to evaluate the CO_2 adsorption capabilities of the catalysts. As shown in Fig. 3c, the CO_2 desorption profiles can be divided into three regions: desorption below 150 °C is attributed to physically adsorbed CO_2, the region between 150 and 450 °C corresponds to moderate adsorption, and the high-temperature region (450–750 °C) is associated with strong adsorption [50,51]. To clarify the origin of the desorption features, a CO_2-TPD experiment was also conducted on pure In_2O_3. As shown in Fig. S11, In_2O_3 exhibits desorption peaks at 310 °C and 437 °C. The peak at 310 °C is assigned to oxygen vacancies generated by H_2 reduction of In_2O_3 [43]. Compared with CoIn-based catalysts, the larger peak area at this position suggests that Co species facilitate H_2 dissociation on the catalyst surface, thereby generating more oxygen vacancies. Notably, the CO_2 adsorption center of CoInZr exhibits significant differences from that of CoIn. CoInZr exhibits not only a higher CO_2 uptake in the weak adsorption region but also distinct desorption peaks around 400 °C and 557 °C. The signal below 150 °C is attributed to bicarbonates formed through interaction with surface hydroxyl species [52]. This phenomenon may be related to the previously reported frustrated Lewis acid-base pair (FLP) sites by our research team [53]. Meanwhile, the peak at 557 °C is assigned to monodentate carbonates resulting from chemical interactions between CO_2 and strong Lewis acid sites introduced by ZrO_2 [41]. Similarly, for CoInCe, large desorption peaks observed near 450 °C and 670 °C suggest that the introduction of CeO_2 enhances CO_2 adsorption. This may be attributed to the unique oxygen

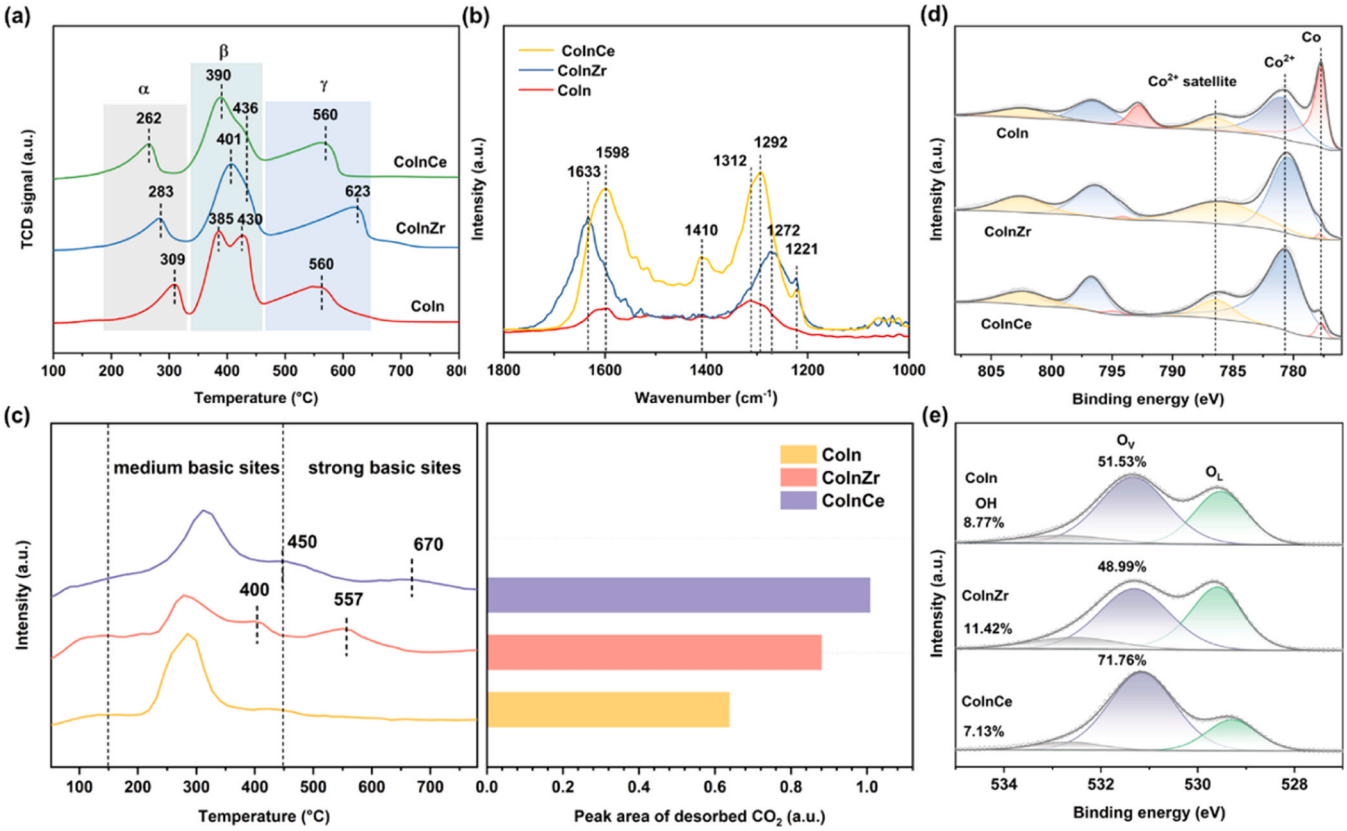

Fig. 3. Characterization of H_2 and CO_2 adsorption and activation properties. (a) H_2-TPR profiles, (b) DRFTIR of CO_2 adsorption, (c) CO_2-TPD profiles and the total CO_2 adsorption capacity, XPS spectroscopy for (d) Co 3d and (e) O 1 s of CoIn, CoInZr and CoInCe.

storage capability and oxygen vacancy formation properties of the Ce component, which effectively increase surface alkalinity [54]. To further compare the concentration of surface basic sites, the quantitative peak areas of desorbed CO_2 were calculated. The total amounts of CO_2 adsorbed on CoInCe and CoInZr are higher than that on CoIn, confirming their superior CO_2 adsorption performance. This trend aligns well with the higher CO_2 conversion observed in CO_2 hydrogenation reactions. Differences in CO_2 adsorption capacity among these catalysts may derive from distinct active phase structures.

To identify the adsorption configuration of CO_2 on the catalyst surface, in situ IR spectroscopy was performed after CO_2 adsorption (Fig. 3b). For both CoIn and CoInCe catalysts, the peaks at 1598 cm^{-1} and 1312 cm^{-1} are attributed to the V_{as}(OCO) and V_s(OCO) in bidentate carbonate (b-CO_3^{2-}), respectively [55]. It is worth noting that bidentate bicarbonate (b-HCO_3^-) (1633, 1272 and 1221 cm^{-1}) is detected only in the CoInZr sample, which is consistent with the results from CO_2-TPD experiments [56,57]. Additionally, signals observed at 1272 cm^{-1}, 1410 cm^{-1}, and 1292 cm^{-1} are assigned to monodentate carbonate (m-CO_3^{2-}), indicating the presence of this carbonate species in all three catalysts [37].

To elucidate the structural changes in the catalyst following the reaction, we conducted X-ray photoelectron spectroscopy (XPS) measurements. The Co 2p spectra exhibit a characteristic asymmetric line shape, with binding energies at approximately 777.8 eV and 780.7 eV corresponding to Co^0 and Co^{2+} species, respectively, indicating the coexistence of metallic Co^0 and oxidized Co^{2+} states in the CoIn, CoInZr, and CoInCe catalysts (Fig. 3d) [58]. Furthermore, the satellite peak at 786.5 eV confirms the formation of a CoO phase, suggesting a reduction process from Co_3O_4 to CoO. The surface Co/In atomic ratio of the spent catalyst consistently exceeds its bulk counterpart (Table S5), consistent with the phase separation observed in HRTEM results. This phenomenon can be attributed to the high mobility of metallic Co atoms, leading to the localized enrichment. Quantitative analysis of the Co^0 fraction was further performed by peak-fitting of the Co 2p spectra. The results reveal that the CoIn catalyst possesses the highest Co^0 content, in agreement with the XRD analysis. In the In 3d XPS region, two broad peaks are observed at 444–445 eV (In $3d_{5/2}$) and 451–452 eV (In $3d_{3/2}$), respectively (Fig. S12). The fitting results indicate the coexistence of In^{3+} and partially reduced $In^{\delta+}$ ($\delta < 3$) species in the CoIn-based catalysts [59]. Notably, the binding energy of In $3d_{5/2}$ follows the order: CoIn > CoInZr > CoInCe, suggesting the formation of more abundant InO_x species in CoInZr and CoInCe. Such InO_x species readily interact with CoO to form CoO-InO_x interfaces on the surface of metallic Co^0 particles. These interfaces are considered to be key active sites for promoting H_2 adsorption.

Electron Paramagnetic Resonance (EPR) measurements and O 1 s XPS spectra were employed to investigate the oxygen vacancies in CoIn-based catalysts. The EPR results indicate that the concentration of oxygen vacancies in the spent catalysts follows the order: CoInCe > CoIn > CoInZr (Fig. S13). Moreover, Fig. 3e displays the O 1 s XPS spectra of the catalysts. The peak at approximately 529.6 eV is attributed to lattice oxygen (O_L), the peak at around 531.3 eV corresponds to oxygen vacancies (O_V), and the peak near 532.7 eV is associated with surface hydroxyl groups (*OH) [20]. The relative abundance of defect-related oxygen species was evaluated by calculating the $O_V/(O_V+O_L+OH)$ ratio. Deconvolution of the Ce 3d XPS spectrum further confirms the coexistence of Ce^{3+} and Ce^{4+} oxidation states in the spent CoInCe catalyst (Fig. S14). Therefore, the abundant oxygen vacancies in CoInCe originate not only from the reduction of In_2O_3 and Co_3O_4 but also from the reduction of CeO_2 [35], which contributes to the richer basic sites observed in CO_2-TPD and consequently promotes CO_2 adsorption and activation. Although the CoInZr catalyst shows a lower O_V concentration than CoIn, it possesses more surface hydroxyl groups, further corroborating the CO_2-TPD results.

2.4. Mechanistic insight

According to our previous studies, In-H species derived from H_2 dissociation on In_2O_3 participate in the subsequent hydrogenation of key intermediates such as HCOO* [53]. Furthermore, Co promotes the dissociation of H_2 onto In_2O_3, thereby facilitating the activation of H_2 [55,60]. Therefore, H_2-TPD was employed to investigate the hydrogen activation ability of the catalysts. As shown in Fig. 4a, with the addition of ZrO_2 andCeO_2, the hydrogen desorption behavior is significantly altered compared to the CoIn catalyst. The H_2 desorption peak areas of the CoInCe and CoInZr catalysts are 4.7 times and 3.2 times larger than that of the CoIn catalyst, respectively, indicating a notable rise in the number of active sites for activating H_2 after doping [61]. In addition, the H_2 desorption temperatures of CoInCe and CoInZr shifts toward lower values, demonstrating that doping with Zr and Ce may generate new active sites that more readily adsorb H_2, thereby promoting methanol formation.

The reaction intermediates and pathways were investigated using *in situ* diffuse reflectance infrared Fourier transform spectroscopy (DRIFTS). When the catalyst was exposed to a CO_2/H_2 reaction atmosphere, CO_2 was rapidly adsorbed on the surface in the form of CO_3^{2-} and HCO_3^- (Fig. 4b, 4c, and S15). After that, new peaks emerged at 1585 cm^{-1}, 1370 cm^{-1}, and 2875 cm^{-1}, which can be assigned to the v_{as} (OCO), v_s (OCO), and C–H vibrations of HCOO*, respectively. In addition, the signal at 1053 cm^{-1} is attributed to CH_3O*. Formic acid pulse experiments detected distinct MS signals for CH_3OH and HCHO (Fig. S16). This suggests that CO_3^{2-}/HCO_3^- species form preferentially during CO_2 hydrogenation and then convert to HCOO*, supporting the formate pathway as the dominant mechanism [55].

The kinetics of surface intermediate conversion were further probed by tracking the dynamic evolution of HCOO* and CH_3O*. As shown in Fig. 4d, the intensity of HCOO*/CH_3O* increased over time until a decrease was observed after approximately 40 min. This phenomenon likely arises because the conversion of HCOO* to CH_3O* is rate-determining, necessitating the accumulation of HCOO* to a threshold level before rapid conversion can proceed [57]. In particular, the slower increase and lower intensity of the HCOO*/CH_3O* ratio within the first 5 min on CoInZr suggests more rapid consumption of HCOO*, pointing to the lowest energy barrier for methanol formation. Conversely, the CoInCe catalyst combines a high energy barrier with high activity, which implies that more complex reaction pathways are involved.

In fact, alongside the formate pathway, reaction pathways forming methanol from CO, a by-product generated by the RWGS reaction, have also been reported [5]. To investigate the possibility of this pathway over the CoInCe catalyst, we conducted CO-TPD experiments (Fig. 4e). The results clearly show that CoInCe exhibits the highest CO adsorption capacity, indicating a greater potential for CO conversion on its surface. In addition, CO-TPSR experiment with pre-adsorbed H_2 was performed on CoInCe. As shown in the Fig. S17, consumption of H_2 and CO was detected by mass spectrometry around 300 °C, accompanied by the formation of HCOOH and CO_2. This suggests that gaseous CO interacts with surface H species at elevated temperatures to generate key intermediates for methanol synthesis.

To further verify this, the catalyst was reduced in the *in-situ* IR cell and then exposed to CO for sufficient adsorption. As shown in the corresponding spectra (Fig. S18), CoInCe displays two characteristic absorption bands of CO. The peaks at 2177 cm^{-1} and 2117 cm^{-1} are assigned to gaseous CO, while those at 2068 cm^{-1} and 2018 cm^{-1} correspond to adsorbed CO species on the surface [62]. It is worth noting that, compared with CoInZr, signals for COOH*, HCOO* and CH_3O* were detected only on CoInCe. This is likely due to the hydrogenation of CO* by active hydrogen species adsorbed at the CoO_x-InO_x interface, suggesting that the reaction mechanism over CoInCe differs from that over CoInZr. Subsequently, to monitor the dynamic evolution of surface species, the CO flow was stopped while maintaining a H_2/Ar atmosphere over the CoInCe catalyst. The time-dependent DRIFTS spectra reveal a

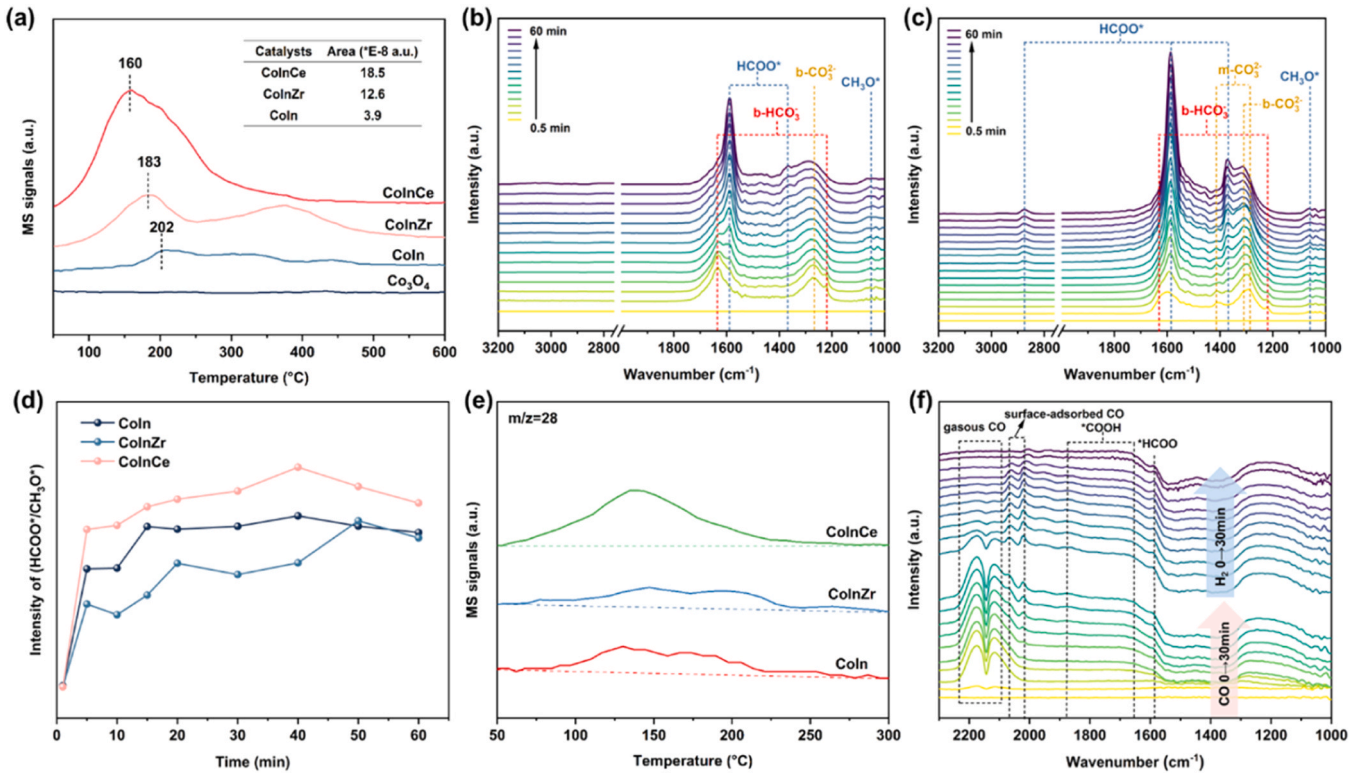

Fig. 4. Characterization and evolution of reactive intermediates. (a) H_2-TPD profile of Co_3O_4, CoIn, CoInZr and CoInCe. In situ DRIFTS spectra of $CO_2 + H_2$ reaction in the range of 1000–3200 cm^{-1} over (b) CoInZr and (c) CoInCe. (d) The ratio of HCOO* to CH_3O* intermediates changes as a function of time. (e) CO-TPD profile of Co_3O_4, CoIn, CoInZr and CoInCe. (f) Time-resolved DRIFTS spectra of CoInZr at 200 °C during alternating H_2 and CO exposure.

gradual consumption of adsorbed CO species accompanied by a continuous increase in the intensity of HCOO* bands (Fig. 4f). When the introduction order of H_2 and CO was reversed, signals corresponding to HCOO* and *COOH were still observed upon CO exposure (Fig. S19). This observation indicates the coexistence of both the formate pathway and the CO pathway over CoInCe, which may explain why this catalyst maintains high methanol selectivity even at elevated temperatures.

3. Conclusions

In summary, this study demonstrated that the incorporation of ZrO_2 and CeO_2 distinctly modulated the catalytic performance and reaction mechanism of CoIn-based catalysts for CO_2 hydrogenation to methanol. CoIn and CoInZr catalysts produce methanol predominantly via the formate intermediate. However, the introduction of ZrO_2 effectively suppresses the reduction of CoO_x, leading to the formation of more CoO_x-InO_x interfacial sites, while simultaneously enhancing the adsorption and activation of CO_2 and H_2. Doping with CeO_2 improves both CO_2 conversion and methanol selectivity. The superior performance of CoInCe is attributed to the unique coexistence of both formate and CO hydrogenation pathways. This dual-pathway mechanism allows CoInCe to maintain high methanol yield even under elevated temperatures. Collectively, this study establishes precise doping as an effective approach for enhancing methanol synthesis by directing the reaction mechanism, offering a clear blueprint for future catalyst development.

CRediT authorship contribution statement

LI Guangchao: Writing – review & editing, Writing – original draft, Supervision, Project administration, Formal analysis. **Christopher Foo:** Writing – review & editing, Writing – original draft, Formal analysis. **Xia Li:** Writing – original draft, Visualization, Methodology, Investigation, Formal analysis, Data curation, Conceptualization. **Xinlin Hong:** Writing – review & editing, Writing – original draft, Supervision, Project administration.

Declaration of Competing Interest

The authors declare no competing financial interest.

Acknowledgements

The financial support from the Hong Kong Polytechnic University (P0049034, P0055259), the Department of Science and Technology of Guangdong Province (GDSTC 2025A1515011688), the Hong Kong Research Grants Council (15301725), the Research Centre for Carbon-Strategic Catalysis (P0058122), the Shenzhen Science and Technology Program (JCYJ20250604185422030), the Research Grants Council Collaborative Research Fund (C5057–24E, C5081–21E) and the National Natural Science Foundation of China (Grants W2541007) is gratefully acknowledged. G. Li gratefully acknowledges support from the University Research Facility in Chemical and Environmental Analysis (UCEA) at PolyU.

This work is dedicated to Professor Shik Chi Edman Tsang, whose invaluable contributions to the global field of heterogeneous catalysis research will be forever cherished and deeply missed.

Appendix A. Supporting information

Supplementary data associated with this article can be found in the online version at doi:10.1016/j.apcata.2026.120976.

Data availability

Data will be made available on request.

References

[1] J. Artz, T.E. Müller, K. Thenert, J. Kleinekorte, R. Meys, A. Sternberg, A. Bardow, W. Leitner, Sustainable conversion of carbon dioxide: an integrated review of catalysis and life cycle assessment, Chem. Rev. 118 (2017) 434–504.

[2] P. Gao, L. Zhong, B. Han, M. He, Y. Sun, Green carbon science: keeping the pace in practice, Angew. Chem. Int. Ed. 61 (2022).

[3] D. Gilfillan, G. Marland, CDIAC-FF: global and national CO_2 emissions from fossil fuel combustion and cement manufacture: 1751-2017, Earth Syst. Sci. Data 13 (2021) 1667–1680.

[4] M. He, Y. Sun, B. Han, Green carbon science: efficient carbon resource processing, utilization, and recycling towards carbon neutrality, Angew. Chem. Int. Ed. 61 (2022) e202112835.

[5] X. Jiang, X. Nie, X. Guo, C. Song, J.G. Chen, Recent advances in carbon dioxide hydrogenation to methanol via heterogeneous catalysis, Chem. Rev. 120 (2020) 7984–8034.

[6] G.A. Olah, Beyond oil and gas: the methanol economy, Angew. Chem. Int. Ed. 44 (2005) 2636–2639.

[7] J. Zhong, X. Yang, Z. Wu, B. Liang, Y. Huang, T. Zhang, State of the art and perspectives in heterogeneous catalysis of CO_2 hydrogenation to methanol, Chem. Soc. Rev. 49 (2020) 1385–1413.

[8] O.-S. Joo, K. Jung, I. Moon, A.Y. Rozovskii, G.I. Lin, S. Han, S. Uhm, Carbon dioxide hydrogenation to form methanol via a reverse-water-gas-shift reaction (the CAMERE process), Ind. Eng. Chem. Res. 38 (1999) 1808–1812.

[9] A.M. Bahmanpour, M. Signorile, O. Kröcher, Recent progress in Syngas production via catalytic CO_2 hydrogenation reaction, Appl. Catal. B Environ. 295 (2021) 120319.

[10] J. Niu, H. Liu, Y. Jin, B. Fan, W. Qi, J. Ran, Comprehensive review of Cu-based CO_2 hydrogenation to CH_3OH: Insights from experimental work and theoretical analysis, Int. J. Hydrog. Energy 47 (2022) 9183–9200.

[11] G. Pacchioni, From CO_2 to methanol on $Cu/ZnO/Al_2O_3$ industrial catalyst. What do we know about the active phase and the reaction mechanism? ACS Catal. 14 (2024) 2730–2745.

[12] P. Gao, F. Li, L. Zhang, N. Zhao, F. Xiao, W. Wei, L. Zhong, Y. Sun, Influence of fluorine on the performance of fluorine-modified Cu/Zn/Al catalysts for CO_2 hydrogenation to methanol, J. CO_2 Util. 2 (2013) 16–23.

[13] L. Song, G. Liu, Z. Qu, Controlling CO_2 hydrogenation selectivity by tuning surface properties of $Cu/Zn_xAl_yO_z$ catalysts, Chem. Eng. J. 494 (2024) 153206.

[14] Y. Jia, Y. Ding, T. Song, Y. Xu, Y. Li, L. Duan, F. Li, L. Sun, K. Fan, Dynamic surface reconstruction of amphoteric metal (Zn, Al) doped Cu_2O for efficient electrochemical CO_2 reduction to C_{2+} products, Adv. Sci. 10 (2023) 2303726.

[15] A. Cherevotan, J. Raj, L. Dheer, S. Roy, S. Sarkar, R. Das, C.P. Vinod, S. Xu, P. Wells, U.V. Waghmare, S.C. Peter, Operando generated ordered heterogeneous catalyst for the selective conversion of CO_2 to methanol, ACS Energy Lett. 6 (2021) 509–516.

[16] Q. Sun, X. Liu, Q. Gu, Z. Sun, H. Wang, L. Cao, Y. Xu, S. Li, B. Yang, S. Wei, J. Lu, Breaking the conversion-selectivity trade-off in methanol synthesis from CO_2 using dual intimate oxide/metal interfaces, J. Am. Chem. Soc. 146 (2024) 28885–28894.

[17] A. Tsoukalou, P.M. Abdala, D. Stoian, X. Huang, M.-G. Willinger, A. Fedorov, C. R. Müller, Structural evolution and dynamics of an In_2O_3 catalyst for CO_2 hydrogenation to methanol: an Operando XAS-XRD and in situ TEM study, J. Am. Chem. Soc. 141 (2019) 13497–13505.

[18] W. Wang, K. Huo, Y. Wang, J. Xie, X. Sun, Y. He, M. Li, J. Liang, X. Gao, G. Yang, S. Lin, F. Cao, H. Jiang, M. Wu, N. Tsubaki, Rational control of oxygen vacancy density in In_2O_3 to boost methanol synthesis from CO_2 hydrogenation, ACS Catal. 14 (2024) 9887–9900.

[19] J. Ye, C. Liu, D. Mei, Q. Ge, Active oxygen vacancy site for methanol synthesis from CO_2 hydrogenation on In_2O_3(110): a DFT study, ACS Catal. 3 (2013) 1296–1306.

[20] Z. Zhou, Y. Wang, Y. Bao, H. Yang, J. Li, C. Chang, S. Li, P. Gao, Nickel-modified In_2O_3 with inherent oxygen vacancies for CO_2 hydrogenation to methanol, Sci. China Chem. 67 (2024) 1715–1728.

[21] N. Rui, Z. Wang, K. Sun, J. Ye, Q. Ge, C. Liu, CO_2 Hydrogenation to methanol over Pd/In_2O_3: effects of Pd and oxygen vacancy, Appl. Catal. B Environ. 218 (2017) 488–497.

[22] M.S. Frei, C. Mondelli, R. García-Muelas, K.S. Kley, B. Puértolas, N. López, O. V. Safonova, J.A. Stewart, D. Curulla Ferré, J. Pérez-Ramírez, Atomic-scale engineering of indium oxide promotion by palladium for methanol production via CO_2 hydrogenation, Nat. Commun. 10 (2019).

[23] K. Sun, N. Rui, Z. Zhang, Z. Sun, Q. Ge, C. Liu, A highly active Pt/In_2O_3 catalyst for CO_2 hydrogenation to methanol with enhanced stability, Green. Chem. 22 (2020) 5059–5066.

[24] M. Li, H. Zou, J. Zheng, T. Wu, T. Chan, Y. Soo, X. Wu, X. Gong, T. Chen, K. Roy, G. Held, S. Tsang, Methanol synthesis at a wide range of H_2/CO_2 ratios over a Rh-In bimetallic catalyst, Angew. Chem. Int. Ed. 59 (2020) 16039–16046.

[25] N. Rui, F. Zhang, K. Sun, Z. Liu, W. Xu, E. Stavitski, S.D. Senanayake, J. A. Rodriguez, C. Liu, Hydrogenation of CO_2 to methanol on a $Au^{\delta+}$-In_2O_{3-x} catalyst, ACS Catal. 10 (2020) 11307–11317.

[26] M. Zhang, H. Chen, K. Cheng, L. Zhao, H. Huang, J. Kang, Q. Zhang, Y. Wang, Reaction-induced formation of CoO_x-InO_x interfaces for the hydrogenation of CO_2 to methanol, J. Phys. Chem. C 129 (2025) 2535–2545.

[27] S. Liu, Y. He, W. Fu, J. Chen, J. Ren, L. Liao, R. Sun, Z. Tang, C. Mebrahtu, F. Zeng, Hetero-site cobalt catalysts for higher alcohols synthesis by CO_2 hydrogenation: a review, J. CO_2 Util. 67 (2023) 102322.

[28] L. Wang, W. Zhang, X. Zheng, Y. Chen, W. Wu, J. Qiu, X. Zhao, X. Zhao, Y. Dai, J. Zeng, Incorporating nitrogen atoms into cobalt nanosheets as a strategy to boost catalytic activity toward CO_2 hydrogenation, Nat. Energy 2 (2017) 869–876.

[29] Y. Fang, F. Wang, Y. Chen, Q. Lv, K. Jiang, H. Yang, H. Zhao, P. Wang, Y. Gan, L. Wu, Y. Tang, X. Gao, L. Tan, Realizing methanol synthesis from CO and water via the synergistic effect of Cu^0/Cu^+ over Cu/ZrO_2 catalyst, J. Energy Chem. 93 (2024) 126–134.

[30] E. Lam, K. Larmier, P. Wolf, S. Tada, O.V. Safonova, C. Copéret, Isolated Zr surface sites on silica promote hydrogenation of CO_2 to CH_3OH in supported Cu catalysts, J. Am. Chem. Soc. 140 (2018) 10530–10535.

[31] K. Li, J.G. Chen, CO_2 hydrogenation to methanol over ZrO_2-containing catalysts: insights into ZrO_2 induced synergy, ACS Catal. 9 (2019) 7840–7861.

[32] C.Y. Regalado Vera, N. Manavi, Z. Zhou, L. Wang, W. Diao, S. Karakalos, B. Liu, K. J. Stowers, M. Zhou, H. Luo, D. Ding, Mechanistic understanding of support effect on the activity and selectivity of indium oxide catalysts for CO_2 hydrogenation, Chem. Eng. J. 426 (2021) 131767.

[33] A. Tsoukalou, P.M. Abdala, A. Armutlulu, E. Willinger, A. Fedorov, C.R. Müller, Operando X-ray absorption spectroscopy identifies a monoclinic ZrO_2: in solid solution as the active phase for the hydrogenation of C_{O2} to methanol, ACS Catal. 10 (2020) 10060–10067.

[34] X. Zhang, A.V. Kirilin, S. Rozeveld, J.H. Kang, G. Pollefeyt, D.F. Yancey, A. Chojecki, B. Vanchura, M. Blum, Support effect and surface reconstruction in In_2O_3/m-ZrO_2 catalyzed CO_2 hydrogenation, ACS Catal. 12 (2022) 3868–3880.

[35] L. Wang, W. Wang, X. Zhang, Y. Zhang, C. Peng, Exploring the influence of morphological variations in M/CeO_2 catalysts for enhanced CO_2 hydrogenation to C_1 products, J. Mater. Chem. A 13 (2025) 19073–19104.

[36] J. Graciani, K. Mudiyanselage, F. Xu, A.E. Baber, J. Evans, S.D. Senanayake, D. J. Stacchiola, P. Liu, J. Hrbek, J.F. Sanz, J.A. Rodriguez, Highly active Copper-ceria and Copper-ceria-titania catalysts for methanol synthesis from CO_2, Science 345 (2014) 546–550.

[37] T. Ke, L. Wang, X. Guo, J. Yu, J. Lang, Y.H. Hu, M. Fan, D. Mao, Two types of catalytic sites of In_2O_3-Co_3O_4/CeO_2 and their synergy for highly selective CO_2 hydrogenation to methanol, Chem. Eng. J. 503 (2025) 158236.

[38] J. Zhu, D. Ciolca, L. Liu, A. Parastaev, N. Kosinov, E.J.M. Hensen, Flame synthesis of Cu/ZnO-CeO_2 catalysts: synergistic metal-support interactions promote CH_3OH selectivity in CO_2 hydrogenation, ACS Catal. 11 (2021) 4880–4892.

[39] C. Shen, K. Sun, R. Zou, Q. Wu, D. Mei, C. Liu, Highly active ternary Ir/In_2O_3-ZrO_2 catalyst for CO_2 hydrogenation towards methanol: the role of zirconia, Appl. Catal. B Environ. Energy 361 (2025) 124683.

[40] X. Jiang, X. Li, S. Xiong, W. Liu, J. Yan, X. Duan, S. Song, Q. Cheng, Y. Tian, X. Li, Synergistical effect of coin alloy and oxygen vacancies over Co-In-Zr ternary catalysts boosting CO_2 hydrogenation to methanol, Carbon Capture Sci. Technol. 14 (2025).

[41] N. Wubulikasimu, R. Shen, L. Hao, H. He, K. Li, X. Li, J. Xie, Selective CO_2 hydrogenation to methanol over a novel ternary In-Co-Zr catalyst, Chem. Eng. J. 501 (2024) 151397.

[42] L. Li, B. Yang, B. Gao, Y. Wang, L. Zhang, T. Ishihara, W. Qi, L. Guo, CO_2 Hydrogenation selectivity shift over In-Co binary oxides catalysts: catalytic mechanism and structure-property relationship, Chin. J. Catal. 43 (2022) 862–876.

[43] O. Martin, A.J. Martín, C. Mondelli, S. Mitchell, T.F. Segawa, R. Hauert, C. Drouilly, D. Curulla-Ferré, J. Pérez-Ramírez, Indium oxide as a superior catalyst for methanol synthesis by CO_2 hydrogenation, Angew. Chem. 128 (2016) 6369–6373.

[44] S. Tada, S. Kayamori, T. Honma, H. Kamei, A. Nariyuki, K. Kon, T. Toyao, K.-i Shimizu, S. Satokawa, Design of interfacial sites between Cu and amorphous ZrO_2 dedicated to CO_2-to-methanol hydrogenation, ACS Catal. 8 (2018) 7809–7819.

[45] S. Feng, X. He, Y. Deng, H. Xu, C. Dun, W. Huang, Unraveling reaction pathways in CO_2 hydrogenation to methanol at metal-oxide interfaces, ACS Catal. 15 (2025) 11981–11992.

[46] N.H.M.D. Dostagir, R. Rattanawan, M. Gao, J. Ota, J. Hasegawa, K. Asakura, A. Fukouka, A. Shrotri, Co single atoms in ZrO_2 with inherent oxygen vacancies for selective hydrogenation of CO_2 to CO, ACS Catal. 11 (2021) 9450–9461.

[47] T. Chen, C. Cao, T. Chen, X. Ding, H. Huang, L. Shen, X. Cao, M. Zhu, J. Xu, J. Gao, Y. Han, Unraveling highly tunable selectivity in CO_2 hydrogenation over bimetallic In-Zr oxide catalysts, ACS Catal. 9 (2019) 8785–8797.

[48] Y. Ge, T. Zou, A.J. Martín, J. Pérez-Ramírez, ZrO_2-promoted Cu-Co, Cu-Fe and Co-Fe catalysts for higher alcohol synthesi, ACS, ACS Catal. 13 (2023) 9946–9959.

[49] C. Yang, C. Pei, R. Luo, S. Liu, Y. Wang, Z. Wang, Z.-J. Zhao, J. Gong, Strong electronic oxide–support interaction over In_2O_3/ZrO_2 for highly selective CO_2 hydrogenation to methanol, J. Am. Chem. Soc. 142 (2020) 19523–19531.

[50] H. Zhang, J. Zhang, S. Yu, D. Wu, Unique interatomic interaction assisted coin intermetallic compound for efficient hydrogenation of CO_2 into methanol, ACS Catal. 15 (2025) 4698–4710.

[51] G. Zhou, H. Liu, Y. Xing, S. Xu, H. Xie, K. Xiong, CO_2 hydrogenation to methane over mesoporous Co/SiO_2 catalysts: effect of structure, J. CO_2 Util. 26 (2018) 221–229.

[52] N.H.M.D. Dostagir, C.R. Tomuschat, K. Oshiro, M. Gao, J. Hasegawa, A. Fukuoka, A. Shrotri, Mitigating the poisoning effect of formate during CO_2 hydrogenation to methanol over Co-containing dual-atom oxide catalysts, JACS Au 4 (2024) 1048–1058.

[53] X. Li, Z. Feng, H. Lu, X. Hong, G. Li, S.C.E. Tsang, Hydroxyl-oxygen vacancy synergy over In_2O_3-ZrO_2 catalysts: mechanistic insights into CO_2 hydrogenation to methanol, J. Mater. Chem. A 13 (2025) 20542–20551.

[54] Y. Guo, L. Jia, Z. Zhang, M. Gong, S. Dang, Y. Huang, X. Gao, W. Tu, Y. Han, Revealing the mechanism of Ce promoter in modulating product distribution of CO_2 hydrogenation over Fe-based catalysts, Chem. Eng. J. 491 (2024) 151964.

[55] S. Dang, W. Zhang, C. Gao, X. Ni, Z. Zhang, W. Tu, Y. Han, Gas-mediated Co single-atom and Co^0 synergy driving CO_2 hydrogenation to methanol over Co/In_2O_3 catalysts, ACS Catal. 15 (2025) 16827–16839.

[56] J. Guo, J. Zheng, D. Meng, A. Zhang, L. Zhou, Z. Wang, The role of dual-interfaces on structural reconstruction of cobalt−zinc−indium catalysts for CO_2 hydrogenation, ACS Catal. 15 (2025) 16893–16907.
[57] K. Pokrovski, K.T. Jung, A.T. Bell, Investigation of CO and CO_2 adsorption on tetragonal and monoclinic zirconia, Langmuir 17 (2001) 4297–4303.
[58] H. Zhang, D. Mao, Jin Zhang, D. Wu, Regulating the crystal structure of layered double hydroxide-derived Co-In catalysts for highly selective CO_2 hydrogenation to methanol, Chem. Eng. J. 452 (2023) 139144.
[59] B. Gao, B. Yang, K. Hatakeyama, Y. Wang, L. Li, S. Ida, T. Ishihara, L. Guo, CO_2 hydrogenation to methanol on $CoIn_2/In_2O_3$: the role of the alloy/oxide interface in driving catalytic activity and selectivity, ACS Catal. 15 (2025) 2305–2314.
[60] S. Dang, X. Nie, Z. Zhang, W. Zhang, J. Li, W. Tu, Strong electronic interaction between In_2O_3 and isolated Co sites enhancing CO_2 hydrogenation to methanol, ACS Sustain. Chem. Eng. 13 (2025) 20287–20297.
[61] X. Jiang, N. Koizumi, X. Guo, C. Song, Bimetallic Pd-Cu catalysts for selective CO_2 hydrogenation to methanol, Appl. Catal. B Environ. 170-171 (2015) 173–185.
[62] S.T. Daniells, A.R. Overweg, M. Makkee, J.A. Moulijn, The mechanism of low-temperature CO oxidation with Au/Fe_2O_3 catalysts: a combined Mössbauer, FT-IR, and TAP reactor study, J. Catal. 230 (2005) 52–65.